Laboratory Investigation (2021) 101:1118–1129
https://doi.org/10.1038/s41374-021-00607-4

ARTICLE

The lncRNA XIST/miR-150-5p/c-Fos axis regulates sepsis-induced myocardial injury via TXNIP-modulated pyroptosis

Xin Wang[1] · Xing-Liang Li[1] · Li-Jie Qin[1]

Received: 28 October 2020 / Revised: 13 April 2021 / Accepted: 15 April 2021 / Published online: 27 May 2021

Abstract

Myocardial injury is a severe complication of sepsis and contributes substantially to the death of critically ill patients. Long non-coding RNAs (lncRNAs) participate in the pathogenesis of sepsis-induced myocardial injury. In this study, we investigated the role of lncRNA X-inactive specific transcript (XIST) in septic myocardial injury and explored its mechanism. Lipopolysaccharide (LPS)-stimulated H9C2 cells and rats subjected to cecal ligation and puncture (CLP) were used as the in vitro and in vivo models. After exposure to LPS, XIST and c-Fos levels were upregulated, but miR-150-5p was downregulated in H9C2 cardiomyocytes and myocardial tissues. XIST affected viability, apoptosis, and pyroptosis in LPS-challenged H9C2 cells. Moreover, XIST knockdown attenuated LPS-induced injury in H9C2 cells by targeting the miR-150-5p/c-Fos axis. c-Fos could bound to the promoter of the *TXNIP/XIST* gene and enhanced TXNIP/XIST expression. Silencing of XIST improved cardiac function and survival rate and reduced apoptosis and pyroptosis by regulating the miR-150-5p/c-Fos axis in septic rats in vivo. Taken together, our data show that XIST/miR-150-5p/c-Fos axis affected septic myocardial injury, which may indicate a novel therapeutic strategy for sepsis-induced myocardial injury.

Introduction

Sepsis is an overwhelming systemic inflammatory response caused by bacterial infection, which is a complication in critically ill patients and may progress to multiple organ dysfunction syndrome. Due to the lack of effective treatment, sepsis is one of the major reasons for the high mortality of hospitalized patients worldwide [1]. Although improvement has been made in therapies for sepsis, its pathogenesis is still not fully understood. Specifically, cardiac insufficiency and even heart failure may occur in septic patients [2]. It has been shown that the mortality rate is 70–90% in septic patients with myocardial dysfunction, higher than that in patients without myocardial injury (20%) [3, 4]. Therefore, for the purpose of improving the outcome and prognosis of sepsis, it is urgent to identify novel and effective therapeutic strategies for sepsis-induced myocardial injury.

✉ Li-Jie Qin
qinlijiee78@163.com

[1] Department of Emergency Medicine, Henan Provincial People's Hospital, Zhengzhou, Henan, PR China

Long non-coding RNAs (lncRNAs) with more than 200 nucleotides have long been regarded as transcriptional noise. Recent studies reveal that lncRNAs regulate gene expression and exert crucial roles in diverse pathological processes, such as the inflammatory response, and tumorigenesis [5–7]. The altered expression of lncRNAs has been verified in sepsis, and participates in the pathogenesis of sepsis-induced myocardial depression [8]. For example, lncRNA NEAT1 silencing attenuated sepsis-induced myocardial injury in rats via suppressing apoptosis and inflammation [9]. Chen et al. suggested that lncRNA MALAT1 exacerbated myocardial inflammation and dysfunction in septic rats through miR-125b and p38/NF-κB pathways [10]. LncRNA X-inactive specific transcript (XIST) expression has been reported to be remarkably increased in septic patients and rats, which took part in sepsis-induced liver injury [11]. However, the effect of XIST on septic myocardial injury remains unclear.

lncRNAs play a crucial biological role through by interacting with microRNAs (miRNAs) and mRNAs. miRNAs consist of 20–25 nucleotides and regulate gene expression by binding to its 3′ untranslated regions (3′UTR) in eukaryotes. They are demonstrated to play extensive pathophysiological roles, such as organ development, cell proliferation, apoptosis, and oncogenesis [12, 13].

Dysregulation of various miRNAs including miR-150, miR-182, miR-584, has been found in the peripheral blood mononuclear cells of septic patients [14]. miRNAs have been recognized as efficient biomarkers for diagnosis and treatment of sepsis. A previous study indicated that XIST may interact with miR-150-5p and regulate hypoxia-induced injury in acute myocardial infarction [15]. However, the regulatory role of XIST-miR-150-5p axis in sepsis-induced myocardial injury remains unclear. In addition, the result of bioinformatics analysis indicated that c-Fos was a potential target of miR-150-5p. Therefore, we speculated that XIST might regulate the progression of septic myocardial injury via the miR-150-c-Fos axis.

In this study, lipopolysaccharide (LPS)-challenged H9C2 cells and rats were used as the in vitro and in vivo septic models to verify whether XIST regulated septic myocardial injury through miR-150-c-Fos axis. Our findings may provide clinical evidence for the prevention and treatment of sepsis-induced myocardial injury.

Materials and methods

Cell culture and treatment

The rat myocardial cell line H9C2 was purchased from the Cell Bank of Chinese Academy of Sciences (Shanghai, China) and cultured in DMEM (Gibco, NY, USA) supplemented with 10% fetal bovine serum (Biological Industries, Israel) at 37 °C with 5% CO_2. To establish the in vitro model of septic myocardial injury, H9C2 cells were stimulated with 1, 5, or 10 μg/mL LPS (Aladdin, Shanghai, China) for 4 h. Afterward, H9C2 cells were collected for further tests.

Vector construction and cell transfection

The miR-150-5p inhibitor and inhibitor netigeve control (NC) were purchased from GenePharma Co., Ltd (Shanghai, China). The H9C2 cells (70–80% confluence) were transfected with these segments using Lipofectamine 2000 (Invitrogen, Carlsbad, CA, USA) following the instructions, respectively. Small hairpin RNA for XIST (sh-XIST), sh-NC was obtained from Shanghai Genepharma Co., Ltd. (Shanghai, China) and this sequence was cloned into the pLKO.1-Puro vector according to the manufacturer's instructions.

Cell counting kit 8 (CCK-8)

After exposure to LPS for 4 h, the viability of H9C2 cells receiving various treatments was assessed with CCK-8 (Beyotime, Haimen, China). In brief, 10 μL of CCK-8 reagent was added to cells seeded into 96-well plate. After incubation for 1 h, the optical density at 490 nm was detected on a microplate reader (Thermo Scientific, Waltham, MA, USA). Cell viability relative to control cells was calculated and shown.

Annexin V-FITC stained FACS

The apoptosis of H9C2 cells subjected to different treatments was analyzed with an Annexin V-FITC Apoptosis Detection Kit (Solarbio, Beijing, China). Briefly, H9C2 cells were harvested, fixed in 70% ethanol, and stained with Annexin V and PI for 15 min away from light. Subsequently, the cells were examined on a flow cytometer (Thermo Scientific).

Animal model

Male Sprague-Dawley rats were acquired from Shanghai SLAC laboratory Animal Co., Ltd.

The polymicrobial sepsis was induced with cecal ligation and puncture (CLP) in rats. Briefly, rats were anesthetized with a gas mixture containing 3% isoflurane and 40% oxygen. A midline surgical incision was performed. The cecum was exposed and ligated by a 3-0 silk suture. The cecum was punctured twice with an 18-gauge needle. Then, the abdomen was closed in layers with 5-0 sutures. For the sham-operated animals, the cecum was mobilized in the absence of CLP. Lentiviral particles were administered through tail veins 1 week before CLP according to a previous study [16]. The rats were randomly assigned to four experimental groups: Sham group ($n = 20$), CLP group ($n = 20$), CLP + sh-NC group ($n = 20$), and CLP + sh-XIST group ($n = 20$). The rats in CLP + sh-NC and CLP + sh-XIST groups were administered with lentiviral particles containing sh-NC or sh-XIST (1×10^9 TU/mL, GenePharma Co., Ltd) through tail veins in a volume of 150 μL. All animal experiments were conducted in accordance with the National Institutes of Health Guidelines for the Care and Use of Laboratory Animals and approved by the Ethics Committee of Henan Provincial People's Hospital.

Cardiac function detection

The cardiac function was evaluated at 2, 6, 24, and 7 d after CLP by echocardiography. Briefly, the rats were anesthetized and determined by short axis M-mode and long axis B-mode echocardiography using the Acuson S3000 imaging system (Siemens, Germany). Using M-mode short axis images, cardiac output (CO) was measured. VevoStrain software was used for myocardial strain analysis of B-mode images.

Table 1 Oligonucleotide primer sets for RT-qPCR.

Name	Sequence (5′ 3′)	Length
XIST F	CGGGTCTCTTCAAGGACATTTAGCC	25
XIST R	GCACCAATACAGAGGAATGGAGGG	24
Fosl2 F	CTCCCGAAGAGGAGGAGAAG	20
Fosl2 R	GGACTGATTTTGCACACAGG	20
GAPDH F	CCAGGTGGTCTCCTCTGA	18
GAPDH R	GCTGTAGCCAAATCGTTGT	19
miR-150-5p F	TCTCCCAACCCTTGTAC	17
miR-150-5p R	GTCGTATCCAGTGCAGGGTCCGAGGT	26
U6 F	CTCGCTTCGGCAGCACATATACT	23
U6 R	ACGCTTCACGAATTTGCGTGTC	22

XIST X-inactive specific transcript, *GAPDH* housekeeping gene glyceraldehyde-3-phosphate dehydrogenase.

HE staining

The collected heart tissues of rats were fixed in 10% formalin, subjected to paraffin embedding, and cut into 5-μm sections. After deparaffinating and rehydration, the sections were successively stained in hematoxylin for 5 min and eosin for 3 min. Afterward, the pathological changes of heart tissues were observed under a light microscope (Olympus).

TUNEL

TUNEL assay was performed to detect the apoptosis in H9C2 cells and myocardial tissues using TUNEL Apoptosis Assay Kit (Solarbio) in accordance with the manufacturer's instructions. Briefly, H9C2 cells or heart tissue sections from different groups were added with 50 μL of TUNEL working solution and incubated at 37 °C for 1 h. After adding with 100 μL reaction buffer, the TUNEL-positive cells were observed under a fluorescence microscope (Olympus, Tokyo, Japan) and quantitatively analyzed with Image J software (National Institutes of Health, Bethesda, MD, USA). The pathologic changes of myocardial tissue in each group were observed under light microscopy. TUNEL-positive nuclei were tested by immunofluorescent method.

ELISA

The IL-1β and IL-18 levels in the supernatant of H9C2 cells and serum were evaluated by the commercial ELISA kits (Boster Biological Technology co. ltd, Wuhan, China) according to the manufacturer's protocols.

Real-time qPCR

Total RNA was isolated from myocardial tissues and H9C2 cells with TRIzol reagent (Thermo Fisher Scientific). Then, reverse transcription into cDNA and RT-qPCR were carried out using the PrimeScript One Step RT-PCR kit (Takara, Osaka, Japan). Table 1 lists the primer sequences used. GAPDH was used as the internal control for XIST and Fosl2, and U6 as internal control for miR-150-5p. $2^{-\Delta\Delta Ct}$ method was employed for relative expression analysis.

Western blotting

The protein levels of c-Fos, NLR-family pyrin domain-containing protein 3 (NLRP3), apoptosis-related speck-like protein containing CARD (ASC), cleaved caspase-1, and thioredoxin-interacting protein (TXNIP) in H9C2 cells and myocardial tissues were assessed by western blotting. In brief, the isolated proteins with a total extraction sample kit (Sigma, Saint Louis, MO, USA) were loaded onto sodium dodecyl sulfate polyacrylamide gel electrophoresis and transferred to polyvinylidene fluoride membranes. Blocking in 5% nonfat milk was performed for 1 h. Afterward, the membranes were probed with primary antibodies c-Fos (1:1000, ab190289, Abcam), NLRP3 (1:1000, ab4207, Abcam), ASC (1:1000, ab111852, Abcam), cleaved Caspase-1 (1:1000, ab2302, Abcam), TXNIP (1:1000, ab188865, Abcam), and GAPDH (1:1000, ab9485, Abcam) at 4 °C overnight. After incubation with the secondary antibodies for 1 h, the membranes were developed using the Super ECL Plus Detection Reagent (Bioss). Protein quantitative analysis was performed using the Gel-Pro-Analyzer software (Media Cybernetics, Bethesda, MD, USA).

Dual-luciferase reporter assay

Luciferase reporter plasmids containing the wild-type (WT) or mutant (MUT) XIST/c-Fos 3′UTR with miR-150-5p binding sites were constructed. Besides, the potential binding sites (BS) for c-Fos within the promoter regions of TXNIP/XIST were identified using JASPAR (http://jaspar.genereg.net/). The different promoter sequences containing WT, or mutated (mut) BS were cloned into a pGL3-basic

vector (Promega, Madison, WI) and transfected into target cells using Lipofectamine 3000 (Invitrogen) according to the manufacturer's instructions. The luciferase activity was detected at 48 h after the transfection using a Dual-Glo Luciferase kit (Promega, Madison, WI, USA).

Chromatin immunoprecipitation (ChIP)

The enrichment of c-Fos with the *TXNIP/XIST* promoter regions was assessed by ChIP using a commercial kit (Millipore). H9C2 cells were incubated with formaldehyde to obtain DNA-protein crosslinks and then lysed. After sonicate treatment, cell lysates were immunoprecipitated with c-Fos (1:20, Abcam) or IgG antibody. The enrichment of TXNIP or XIST in precipitated DNA-protein complexes by Agarose/Sepharose was determined by RT-qPCR.

Statistical analysis

All data are expressed as mean ± standard deviation (SD) and analyzed with SPSS 22.0 software. Comparisons were analyzed by Student's *t* test between two groups, and one-way analysis of variance followed by Tukey's post hoc test among various groups. $P < 0.05$ was considered statistically significant.

Results

Expression of XIST, c-Fos, and miR-150-5p in LPS-induced H9C2 cells

We performed CCK-8 assay to evaluate the viability of H9C2 cells exposure to various concentrations of LPS for 4 h. As shown in Fig. 1A, the viability of H9C2 cells was significantly decreased with the increase of LPS concentration. In addition, LPS challenge triggered apoptosis of H9C2 cells in a dose-dependent manner as detected on a flow cytometer (Fig. 1B). Furthermore, LPS dose-dependently induced apoptosis in H9C2 cells as verified by TUNEL assay (Fig. 1C). As shown in Fig. 1D, the levels of IL-1β and IL-18 in the supernatant of H9C2 were strikingly raised with the increasing concentration of LPS. Therefore, the in vitro model of septic cardiomyocyte injury was successfully established. Moreover, we performed RT-qPCR to determine the expression of XIST and miR-150-5p in H9C2 cells. As presented in Fig. 1E, LPS dose-dependently increased XIST level, but decreased miR-150-5p level in H9C2 cells. As assessed by western blotting, the protein levels of c-Fos, NLRP3, ASC, cleaved caspase-1, TXNIP were upregulated after LPS administration in a dose-dependent manner (Fig. 1F). Thus, the expression of XIST and c-Fos was increased, while miR-150-5p expression was decreased in the in vitro model of septic cardiomyocyte injury.

XIST contributes to LPS-induced cardiomyocyte injury via pyroptosis activation in vitro

Next, the role of XIST in LPS-induced cardiomyocyte injury was investigated via XIST plasmid-mediated overexpression of XIST or sh-XIST-mediated silencing of XIST in H9C2 cells. According to the above results, 5 μg/mL LPS was selected for further experiments. As shown in Fig. 2A, the expression of XIST was verified by RT-qPCR. As assessed by CCK-8, LPS-mediated proliferation inhibition was strengthened by XIST overexpression, but partly reversed by XIST knockdown (Fig. 2B). In addition, the enhanced apoptosis in LPS-challenged H9C2 cells was further promoted by XIST overexpression, while counteracted by silencing of XIST (Fig. 2C, D). As presented in Fig. 2E, overexpression of XIST intensified LPS-induced pyroptosis as evidenced by enhanced secretion of IL-1β and IL-18 in H9C2 cells. However, silencing of XIST presented the opposite results. Besides, LPS-mediated upegulation of c-Fos, NLRP3, ASC, cleaved caspase-1, and TXNIP levels was reinforced in XIST-overexpressed H9C2 cells, but abolished in XIST-silenced cells (Fig. 2F). These findings suggested that XIST regulated LPS-induced cardiomyocyte injury in vitro.

XIST regulates LPS-induced cardiomyocyte injury by affecting pyroptosis via miR-150-5p/c-Fos axis

To further illuminate the mechanisms of XIST in LPS-induced cardiomyocyte injury, we focused on miR-150-5p/c-Fos axis. As illustrated in Fig. 3A, the expression of miR-150-5p was further reduced by XIST overexpression, but enhanced by silencing of XIST in LPS-challenged H9C2 cells. On the contrary, Fosl2 mRNA expression was increased in XIST-overexpressed H9C2 cells, while cut down in XIST-silenced cells upon stimulation with LPS (Fig. 3B). Subsequently, the interaction between miR-150-5p and XIST/Fosl2 in H9C2 cells was investigated. The binding sites for XIST/Fosl2 and miR-150-5p were presented in Fig. 3C, D. Furthermore, miR-150-5p mimics significantly reduced the relative luciferase activity in WT XIST/Fosl2 group but did not affect that in MUT XIST/Fosl2 group (Fig. 3E). Therefore, miR-150-5p could directly bind to XIST/Fosl2 in H9C2 cells. As illustrated in Fig. 3F, the proliferation promoting effect of XIST silencing in LPS-stimulated H9C2 cells was remarkably inhibited by miR-150-5p inhibitor. Additionally, XIST knockdown mediated the inhibition of apoptosis in H9C2 cells exposure to LPS was significantly reversed by miR-150-5p inhibitor (Fig. 3G). Moreover, the suppression of

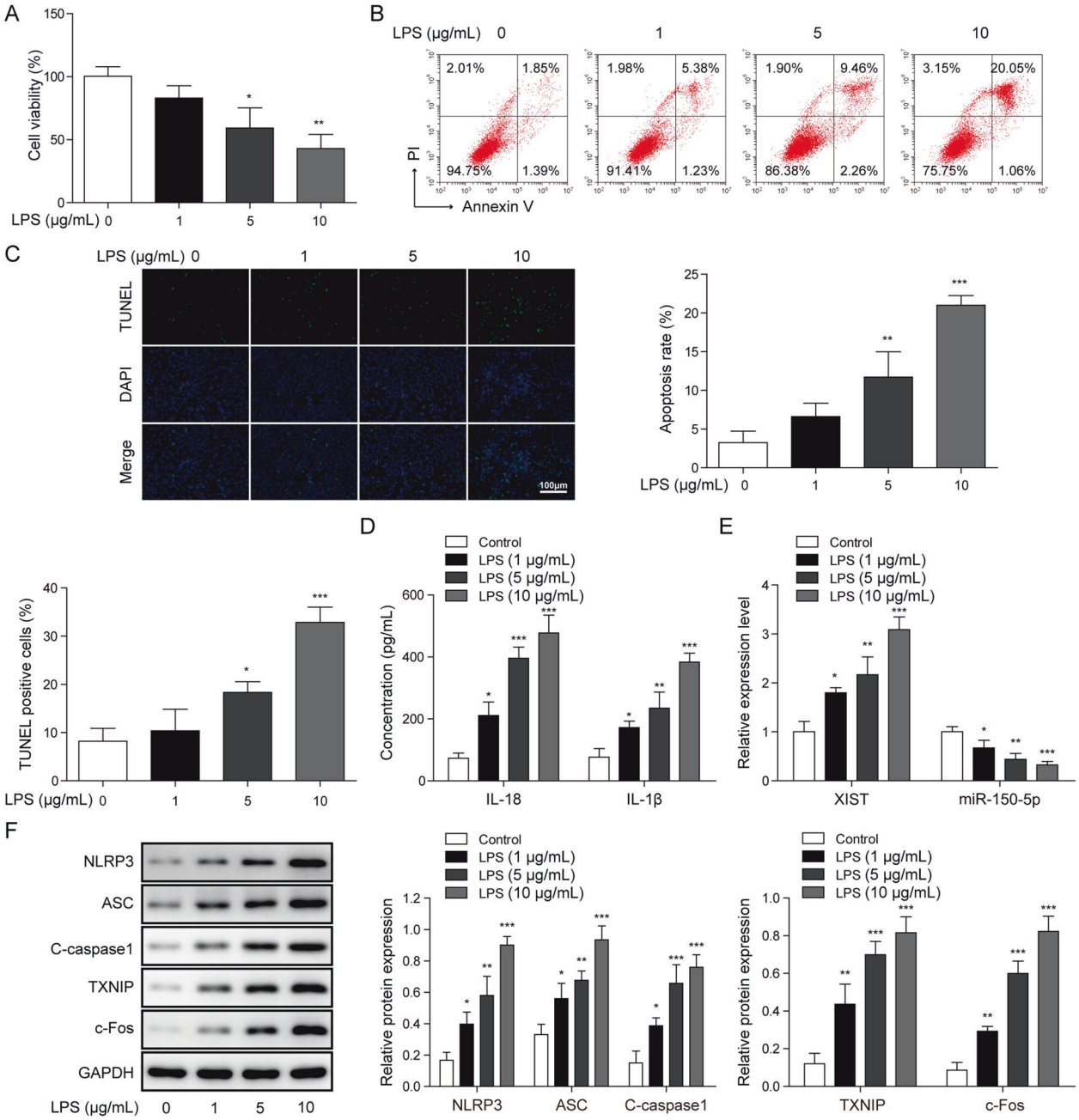

Fig. 1 Expression of XIST, c-Fos, and miR-150-5p in LPS-induced H9C2 cells. H9C2 cells were added with 0, 1, 5, or 10 μg/mL LPS for 4 h. **A** The viability of H9C2 cells was detected by CCK-8 assay. The apoptosis of H9C2 cells was evaluated by Annexin V/PI staining (**B**) and TUNEL staining (**C**). **D** The levels of pro-inflammatory cytokines IL-1β and IL-18 in the supernatant of H9C2 cells were determined by ELISA kits. **E** The expression of XIST and miR-150-5p in H9C2 cells was evaluated by RT-qPCR. **F** Western blotting was carried out to assess the protein levels of c-Fos, NLRP3, ASC, cleaved caspase-1, and TXNIP in H9C2 cells. Data are expressed as mean ± SD ($n = 3$). $^{*}P < 0.05$, $^{**}P < 0.01$, $^{***}P < 0.001$ vs. control group.

pyroptosis after silencing of XIST in LPS-challenged H9C2 cells was reversed by miR-150-5p inhibitor as confirmed by promoting production of IL-1β and IL-18 and enhancing c-Fos, NLRP3, ASC, cleaved caspase-1, and TXNIP levels (Fig. 3H, I). Notably, miR-150-5p inhibitor counteracted XIST knockdown-mediated down-regulation of c-Fos (Fig. 3I). We concluded that XIST influenced LPS-induced cardiomyocyte injury by regulating pyroptosis via miR-150-5p/c-Fos axis.

c-Fos binds to the promoter of *TXNIP* gene

Next, we sought to explore the downstream regulatory mechanisms of c-Fos in septic myocardial injury. As shown

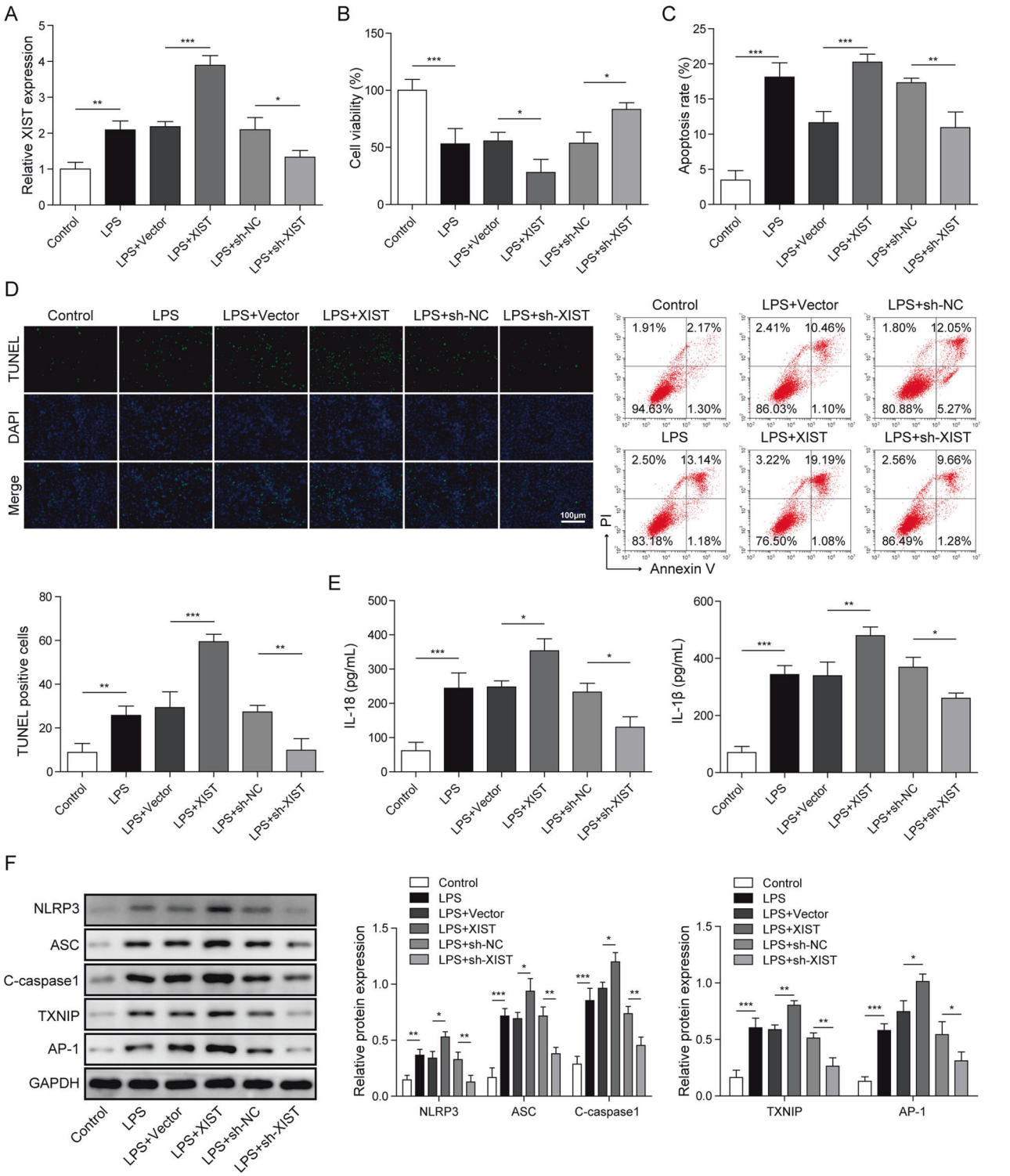

Fig. 2 Effect of XIST on LPS-induced cardiomyocyte injury in vitro. H9C2 cells were transfected with XIST-overexpression plasmid or sh-XIST, and then challenged with 5 μg/mL LPS for 4 h. **A** The expression of XIST in H9C2 cells was detected by RT-qPCR. **B** The viability of H9C2 cells was assessed by CCK-8 assay. The apoptosis of H9C2 cells was determined by Annexin V/PI staining (**C**) and TUNEL staining (**D**). **E** IL-1β and IL-18 levels in the supernatant of H9C2 cells were determined by ELISA kits. **F** Western blotting for determining c-Fos, NLRP3, ASC, cleaved caspase-1, and TXNIP protein levels. Data are expressed as mean ± SD ($n = 3$). $^{*}P < 0.05$, $^{**}P < 0.01$, $^{***}P < 0.001$ vs. control, vector, or sh-NC group.

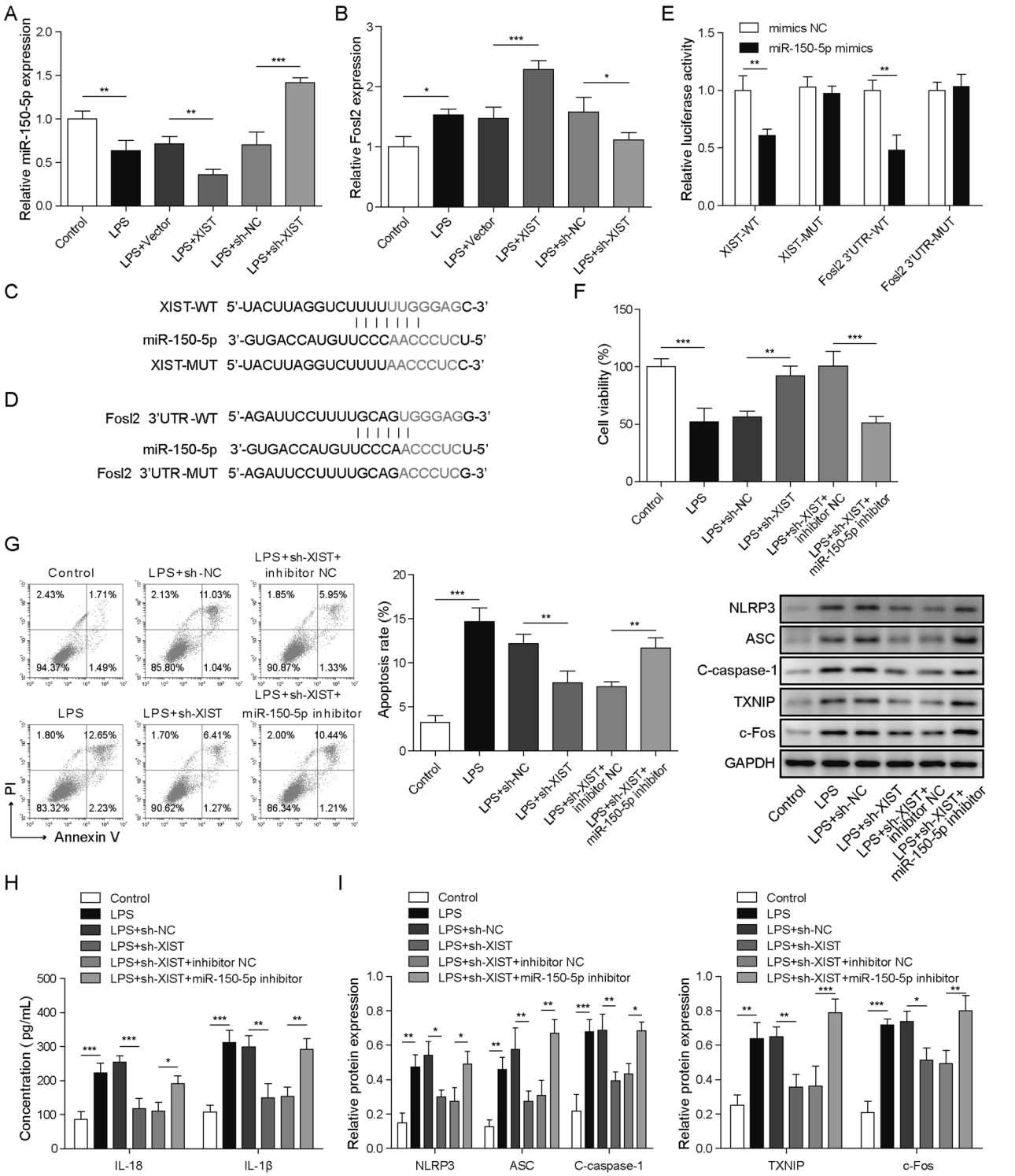

Fig. 3 XIST regulates LPS-induced cardiomyocyte injury via miR-150-5p/c-Fos axis. H9C2 cells were transfected with XIST-overexpression plasmid or sh-XIST, and then challenged with 5 μg/mL LPS for 4 h. **A**, **B** The expression of miR-150-5p and Fosl2 in H9C2 cells was detected by RT-qPCR. **C**, **D** The binding sites for miR-150-5p in XIST/Fosl2 sequence were shown. **E** The interaction between miR-150-5p and XIST/Fosl2 was validated by dual-luciferase reporter assay. H9C2 cells were transfected with sh-XIST or combination with miR-150-5p inhibitor, and then challenged with 5 μg/mL LPS for 4 h. **F** The viability of H9C2 cells were detected by CCK-8 assay. **G** The apoptosis of H9C2 cells was assessed by Annexin V/PI staining. **H** IL-1β and IL-18 levels in the supernatant of H9C2 cells were determined by ELISA kits. **I** The protein levels of c-Fos, NLRP3, ASC, cleaved caspase-1, and TXNIP in H9C2 cells were evaluated by western blotting assay. Data are expressed as mean ± SD ($n = 3$). $^{*}P < 0.05$, $^{**}P < 0.01$, $^{***}P < 0.001$ vs. the indicated group.

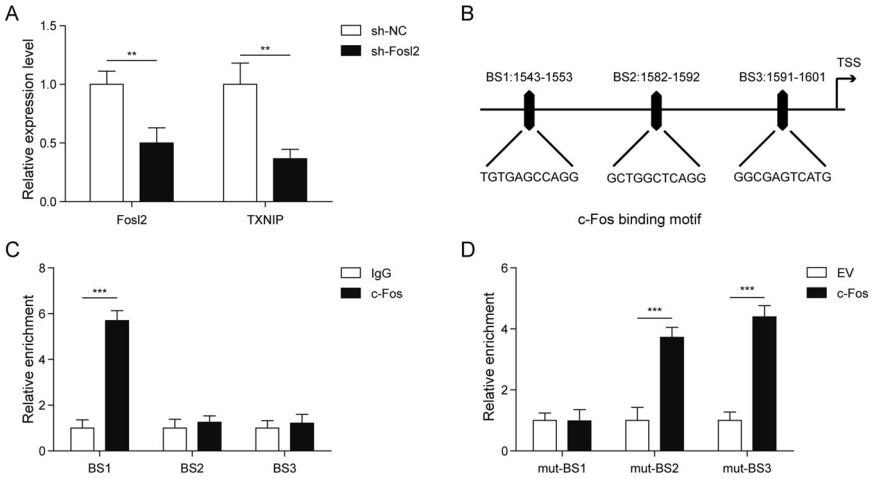

Fig. 4 c-Fos directly activates the transcription of TXNIP. A The expression of Fosl2 and TXNIP in H9C2 cells was detected by RT-qPCR after knockdown of Fosl2. **B** JASPAR analysis identified three potential binding sites (BS1, BS2, and BS3) to c-Fos within the promoter region of TXNIP. **C** The occupancy of c-Fos on the three BSs within TXNIP promoter from indicated cells were determined by ChIP analysis and presented as a fold value relative to the amount of IgG bound to the promoter. **D** The three potential c-Fos binding sequences were mutated and cloned upstream of the reporter. The effect of overexpressing c-Fos on reporter activity was examined by luciferase reporter assay. Data are expressed as mean ± SD ($n = 3$). $^{**}P < 0.01$, $^{***}P < 0.001$.

in Fig. 4A, knockdown of Fosl2 remarkably reduced the mRNA expression of Fosl2 and TXNIP. As predicted by JASPAR database, there were three potential binding sites (BS) between c-Fos and the promoter of TXNIP (Fig. 4B). ChIP assay further demonstrated that c-Fos could bind to the BS1 promoter of TXNIP, but not BS2 and BS3 (Fig. 4C). Besides, the luciferase activity of MUT-BS1 group was not changed after overexpression of c-Fos, whereas the luciferase activities of MUT-BS2 and MUT-BS3 were significantly enhanced (Fig. 4D). These results suggested that c-Fos functioned as a transcriptional factor of TXNIP via binding to the BS1 promoter.

Effect of XIST on myocardial injury in CLP-induced septic rats

We further validated the role of XIST in myocardial injury in CLP-induced sepsis. As presented in Fig. 5A, at 2, 4, 6, 12, and 24 h after CLP surgery, cardiac output (CO) and myocardial strain were significantly reduced, however, this reduction could be attenuated by XIST silencing. Consistently, CLP-induced apoptosis in myocardial tissues was alleviated by XIST knockdown (Fig. 5B). The serious structural damage and inflammatory cell infiltration in myocardial tissues of septic rats could be relieved by XIST depletion (Fig. 5C). CLP surgery resulted in a significant increase in IL-1β and IL-18 levels, which could be abolished by XIST silencing (Fig. 5D). The increase in XIST level in myocardial and liver tissues and reduction in miR-150-5p level in myocardial tissues induced by CLP were reversed by sh-XIST (Fig. 5E). Moreover, XIST silencing counteracted the increase in c-Fos, NLRP3, ASC, cleaved caspase-1, and TXNIP levels in the myocardial tissues of septic rats (Fig. 5F). Similarly, the declined survival rate after CLP surgery was significantly improved by XIST silencing (Fig. 5G). Therefore, XIST knockdown could relieve CLP-induced septic myocardial injury in vivo.

c-Fos contributes to XIST expression via binding to the promoter of XIST

To further investigate how sepsis upregulated XIST, we focused on c-Fos. As illustrated in Fig. 6A, a significant reduction in XIST expression was induced by depletion of Fosl2. JASPAR database indicated there were three potential BS between c-Fos and XIST promoter (Fig. 6B). ChIP assay and dual-luciferase reporter assay further revealed that c-Fos could bind to the BS1 promoter of XIST, but not BS2 and BS3 (Fig. 6C, D). These results indicated that sepsis-induced c-Fos expression could contribute to XIST expression via binding to its BS1 promoter.

Discussion

Sepsis is caused by serious infection and leads to subsequent systemic inflammatory disorders and multiple organ dysfunction syndrome. Myocardial injury is one of the most dangerous complications of sepsis. The interaction of multiple genes is involved in the progression of sepsis-induced myocardial dysfunction [9, 17]. It is imperative to further elucidate the molecular mechanisms of sepsis-induced

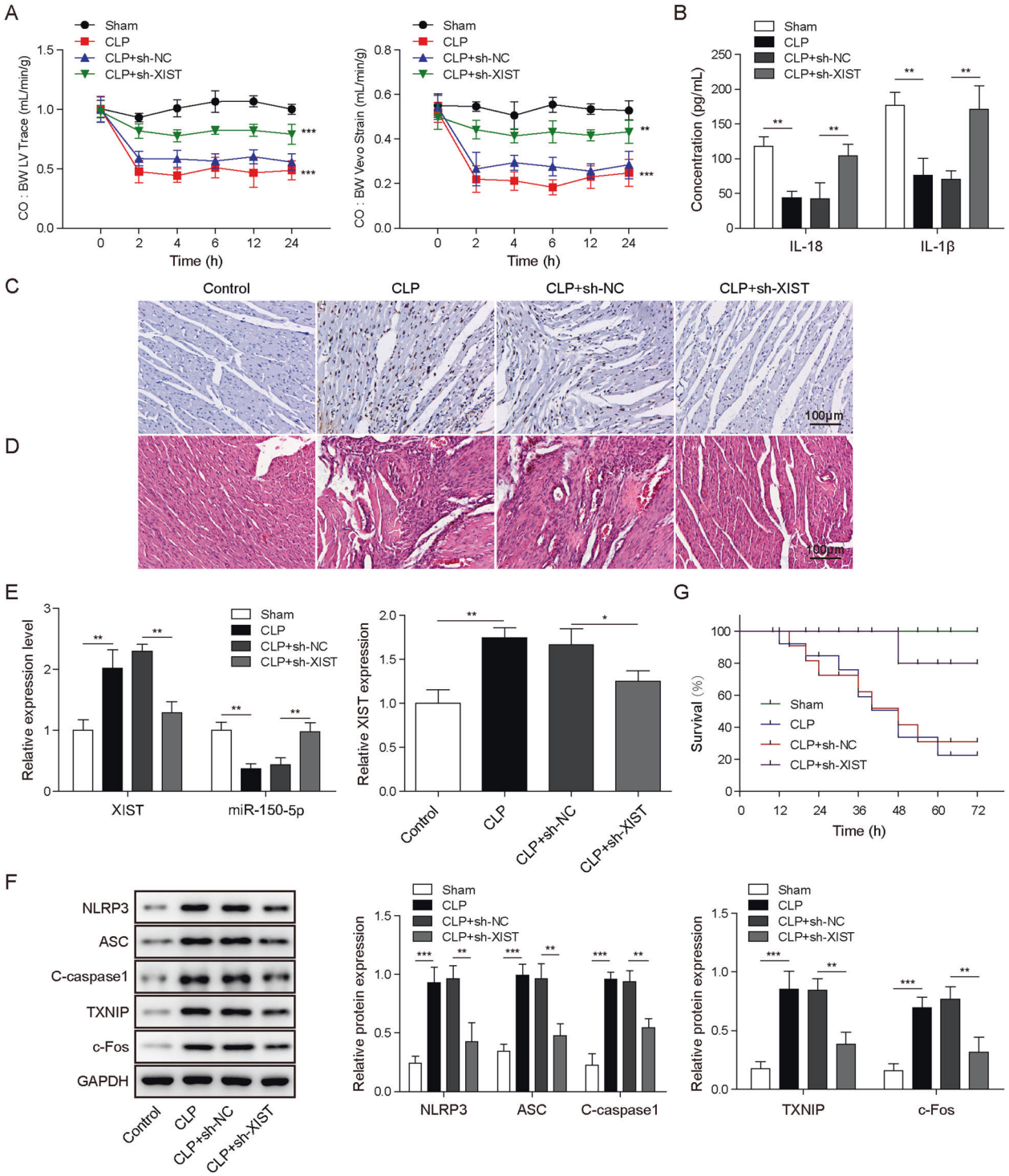

Fig. 5 Knockdown of XIST relieves myocardial injury in CLP-induced septic rats in vivo. The rats were injected with lentiviral particles containing sh-NC or sh-XIST via tail veins, and subjected to CLP 1 week later. **A** cardiac output (CO) and myocardial strain were detected at 2, 4, 6, 24 h after CLP surgery. **B** TUNEL assay for evaluating apoptosis in the myocardial tissues. **C** The pathological changes in the myocardial tissues were detected by HE staining. **D** The serum levels of IL-1β and IL-18 were assessed by ELISA kits. **E** RT-qPCR for the expression of XIST and miR-150-5p in the myocardial or liver tissues. **F** Western blotting for determining the protein levels of c-Fos, NLRP3, ASC, cleaved caspase-1, and TXNIP in the myocardial tissues. **G** The survival rates of rats were monitored every 12 h for up to 72 h after CLP surgery. Data are expressed as mean ± SD ($n = 6$ for A-F, $n = 20$ for **G**). $^{**}P < 0.01$, $^{***}P < 0.001$ vs. sham or CLP + sh-NC group.

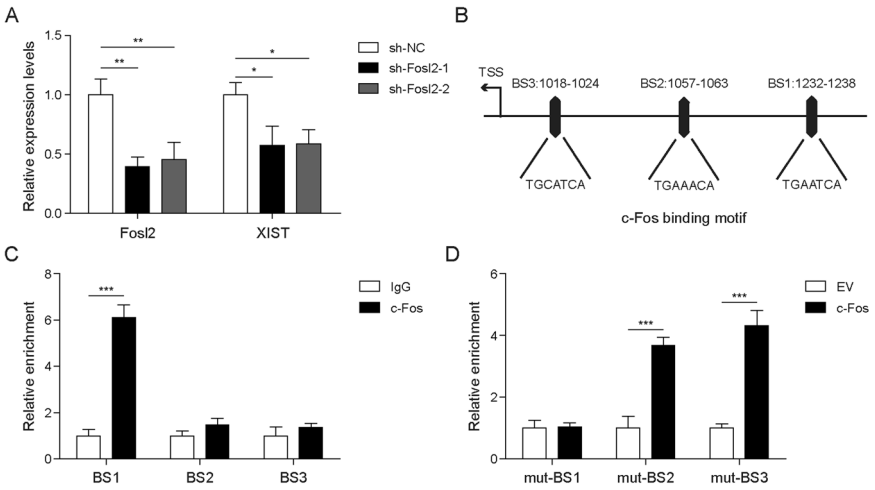

Fig. 6 c-Fos contributes to the transcription of XIST. A RT-qPCR for measuring the expression of Fosl2 and XIST in H9C2 cells. **B** JASPAR analysis predicted three potential binding sites (BS1, BS2, and BS3) to c-Fos within XIST promoter. **C** ChIP analysis for evaluating the binding of c-Fos to the XIST promoter. **D** Three potential c-Fos binding sequences were mutated and cloned upstream of the reporter gene. The effect of overexpressing c-Fos on reporter activity was detected by luciferase reporter assay. Data are expressed as mean ± SD ($n = 3$). $^{*}P < 0.05$, $^{**}P < 0.01$, $^{***}P < 0.001$.

myocardial injury and develop novel therapeutic targets. In this study, we focused on the role of XIST-miR-150-5p-c-Fos axis in septic myocardial injury. The levels of XIST and c-Fos were significantly increased, while miR-150-5p level was decreased in LPS-challenged H9C2 cells in vitro and in the myocardial tissues of septic rats in vivo. XIST regulated septic myocardial injury in vitro and in vivo. Mechanically, XIST functioned as a sponge of miR-150-5p to regulate c-Fos expression and then affected pyroptosis pathway, which participated in the pathogenesis of septic myocardial injury.

It has been well documented that XIST plays pivotal roles in various pathological processes, such as septic kidney injury [18], rheumatoid arthritis [19] and myocardial hypertrophy [20]. Zhou et al. demonstrated that XIST facilitated myocardial infarction by regulating miR-130a-3p [21]. A previous study suggested that XIST was upregulated in sepsis-related lever injury [11]. Therefore, we speculated that XIST might also play a role during the progression of sepsis-induced myocardial injury. In the present study, our results show that XIST expression was increased in H9C2 cells exposed to LPS and myocardial tissues of septic rats. Furthermore, silencing of XIST improved cell viability, restrained apoptosis and pyroptosis in LPS-stimulated H9C2 cells. Overexpression of XIST reversed these effects. In addition, we established a model of septic myocardial injury in rats to verify the above results in vivo. As expected, knockdown of XIST improved cardiac function, suppressed apoptosis and pyroptosis. These findings indicate that XIST was involved in sepsis-induced myocardial injury and might serve as a potential therapeutic target.

XIST has been shown to exert its biological functions via directly binding to miRNAs. For example, Li et al. demonstrated that XIST accelerated the progression of colorectal cancer via targeting miR-338-3p [22]. Similar interaction between XIST and miR-142-5p has been reported in the malignant progression of non-small cell lung cancer [23]. MiR-150-5p is a target gene of XIST, which participates in the pathogenesis of neuropathic pain [24]. Consistently, in our study, XIST could specifically bind to miR-150-5p and regulate its expression in H9C2 cells. Additionally, XIST silencing-mediated improvement in proliferation and pyroptosis inhibition in LPS-challenged H9C2 cells were partly counteracted by miR-150-5p inhibitor. Thus, XIST regulates LPS-induced cardiomyocyte injury by binding to miR-150-5p.

Fosl2 gene encodes c-Fos protein that together with c-Jun forms the transcription factor complex AP-1 in nucleus. c-Fos has been implicated in human cytomegalovirus reactivation [25] osteosarcoma [26], and nervous system development [27]. A previous study found the activation of AP-1 in the ischemic myocardium of rabbits [28]. Zhu et al. demonstrated that c-Fos activation participated in the induction of cardiomyocyte apoptosis [29]. More importantly, c-Fos has been verified as a target gene of miR-150-5p [29]. Using bioinformatics databases, we found that both XIST and c-Fos contain binding sites for miR-150-5p. We therefore speculated that XIST functions as a competing endogenous RNA (ceRNA) to regulate c-Fos expression by binding miR-150-5p. As expected, our data showed that c-Fos was a target of miR-150-5p in H9C2 cells. In addition, c-Fos expression could be increased by XIST

overexpression, but reduced by XIST silencing in LPS-challenged H9C2 cells. XIST was shown to protect target c-Fos from repression by acting as miR-150-5p sponge, revealing the post-transcriptional regulatory role of XIST. Therefore, XIST silencing attenuated septic cardiomyocyte injury by reducing c-Fos expression by binding to miR-150-5p.

To further elucidate the downstream mechanisms of c-Fos in sepsis-induced myocardial injury, TXNIP-mediated pyroptosis was focused on. Fosl2 gene encodes c-Fos protein that forms the transcription factor complex AP-1 in nucleus. As predicted by JASPAR database, there were three potential binding sites between AP-1 (c-Fos) and the promoter of TXNIP. Pyroptosis is a process of programmed cell death attended by overwhelming inflammatory cascade [30]. Mountainous evidence has suggested that pyroptosis takes part in sepsis-induced myocardial injury [31, 32]. Caspase-1 activation can mediate pyroptosis via stimulating NLRP3 inflammasome [33]. In response to NLRP3 inflammasome activation, mature IL-1β and IL-18 are released, which initiate subsequent inflammatory process [34]. It has been recognized that TXNIP can bind to NLRP3 to result in NLRP3 inflammasome activation [35]. Therefore, c-Fos might affect TXNIP-mediated pyroptosis. Interestingly, we verified the binding between c-Fos and TXNIP promoter by ChIP and dual-luciferase reporter assays. Furthermore, silencing of Fosl2 suppressed TXNIP expression in H9C2 cells. These findings indicate that miR-150-5p/c-Fos/TXNIP-mediated pyroptosis was involved in the regulatory mechanisms of XIST in septic myocardial injury.

A recent study by Liang et al. showed that silencing of XIST expression attenuated LPS-induced reduced PGC-1α and Tfam expression, and decreased ATP levels in mouse cardiomyocytes MCM cells [36]. This suggests that repressing XIST expression may improve the metabolic complications of sepsis in our rescue model. We are aware of the fact that there are still some limitations in this study. The underlying mechanism of XIST in regulating metabolic markers remains unclear. Whether XIST/miR-150-5p/c-Fos axis is association with reduced metabolic markers in septic myocardial injury needs to be explored in the future.

In conclusion, our findings demonstrate that silencing of XIST protects against sepsis-induced myocardial injury via regulating miR-150-5p/c-Fos/TXNIP axis. Our results suggest that XIST may serve as a promising therapeutic target for septic myocardial injury.

Data availability

All data generated or analyzed during this study are included in this published article.

Author contributions XW: guarantor, concepts, design, experimental studies, data analysis, preparation, editing; X-LL: experimental studies, data acquisition, data analysis; L-JQ: guarantor, experimental studies, review.

Funding None.

Compliance with ethical standards

Conflict of interest The authors declare no competing interests.

Ethics approval/consent to participate All animal experiments were conducted in accordance with the National Institutes of Health Guidelines for the Care and Use of Laboratory Animals and approved by the Ethics Committee of Henan Provincial People's Hospital and the People's Hospital of Zhengzhou University.

References

1. Vincent JL, Rello J, Marshall J, Silva E, Anzueto A, Martin CD, et al. International study of the prevalence and outcomes of infection in intensive care units. JAMA. 2009;302:2323–9.
2. Lv X, Wang H. Pathophysiology of sepsis-induced myocardial dysfunction. Mil Med Res. 2016;3:30.
3. Romero-Bermejo FJ, Ruiz-Bailen M, Gil-Cebrian J, Huertos-Ranchal MJ. Sepsis-induced cardiomyopathy. Curr Cardiol Rev. 2011;7:163–83.
4. Hochstadt A, Meroz Y, Landesberg G. Myocardial dysfunction in severe sepsis and septic shock: more questions than answers? J Cardiothorac Vasc Anesth. 2011;25:526–35.
5. Lu Q, Meng Q, Qi M, Li F, Liu B. Shear-Sensitive lncRNA AF131217.1 Inhibits Inflammation in HUVECs via Regulation of KLF4. Hypertension. 2019;73:e25–34.
6. Wu XS, Wang F, Li HF, Hu YP, Jiang L, Zhang F, et al. LncRNA-PAGBC acts as a microRNA sponge and promotes gallbladder tumorigenesis. EMBO Rep. 2017;18:1837–53.
7. Meng XD, Yao HH, Wang LM, Yu M, Shi S, Yuan ZX, et al. Knockdown of GAS5 inhibits atherosclerosis progression via reducing EZH2-mediated ABCA1 transcription in ApoE(-/-) mice. Mol Ther Nucleic Acids. 2019;19:84–96.
8. Zhang TN, Goodwin JE, Liu B, Li D, Wen R, Yang N, et al. Characterization of long noncoding RNA and mRNA profiles in sepsis-induced myocardial depression. Mol Ther Nucleic Acids. 2019;17:852–66.
9. Wang SM, Liu GQ, Xian HB, Si JL, Qi SX, Yu YP. LncRNA NEAT1 alleviates sepsis-induced myocardial injury by regulating the TLR2/NF-kappaB signaling pathway. Eur Rev Med Pharmacol Sci. 2019;23:4898–907.
10. Chen H, Wang X, Yan X, Cheng X, He X, Zheng W. LncRNA MALAT1 regulates sepsis-induced cardiac inflammation and dysfunction via interaction with miR-125b and p38 MAPK/NFkappaB. Int Immunopharmacol. 2018;55:69–76.
11. Shen C, Li J. LncRNA XIST silencing protects against sepsis-induced acute liver injury via inhibition of BRD4 expression. Inflammation. 2021;44:194–205.
12. Wang Y, Tai Q, Zhang J, Kang J, Gao F, Zhong F, et al. MiRNA-206 inhibits hepatocellular carcinoma cell proliferation and migration but promotes apoptosis by modulating cMET expression. Acta Biochim Biophys Sin. 2019;51:243–53.

13. Rahmanian S, Murad R, Breschi A, Zeng W, Mackiewicz M, Williams B, et al. Dynamics of microRNA expression during mouse prenatal development. Genome Res. 2019;29:1900–9.
14. Zhou J, Chaudhry H, Zhong Y, Ali MM, Perkins LA, Owens WB, et al. Dysregulation in microRNA expression in peripheral blood mononuclear cells of sepsis patients is associated with immunopathology. Cytokine. 2015;71:89–100.
15. Zhou J, Li D, Yang BP, Cui WJ. LncRNA XIST inhibits hypoxia-induced cardiomyocyte apoptosis via mediating miR-150-5p/Bax in acute myocardial infarction. Eur Rev Med Pharmacol Sci. 2020;24:1357–66.
16. Chen X, Ge W, Hu J, Dong T, Yao H, Chen L, et al. Inhibition of prostaglandin E2 receptor 4 by lnc000908 to promote the endothelial-mesenchymal transition participation in cardiac remodelling. J Cell Mol Med. 2019;23:6355–67.
17. Fang Y, Hu J, Wang Z, Zong H, Zhang L, Zhang R, et al. LncRNA H19 functions as an Aquaporin 1 competitive endogenous RNA to regulate microRNA-874 expression in LPS sepsis. Biomed Pharmacother. 2018;105:1183–91.
18. Xu G, Mo L, Wu C, Shen X, Dong H, Yu L, et al. The miR-15a-5p-XIST-CUL3 regulatory axis is important for sepsis-induced acute kidney injury. Ren Fail. 2019;41:955–66.
19. Wang ZQ, Xiu DH, Jiang JL, Liu GF. Long non-coding RNA XIST binding to let-7c-5p contributes to rheumatoid arthritis through its effects on proliferation and differentiation of osteoblasts via regulation of STAT3. J Clin Lab Anal. 2020;34:e23496.
20. Xiao L, Gu Y, Sun Y, Chen J, Wang X, Zhang Y, et al. The long noncoding RNA XIST regulates cardiac hypertrophy by targeting miR-101. J Cell Physiol. 2019;234:13680–92.
21. Zhou T, Qin G, Yang L, Xiang D, Li S. LncRNA XIST regulates myocardial infarction by targeting miR-130a-3p. J Cell Physiol. 2019;234:8659–67.
22. Li W, He Y, Cheng Z. Long noncoding RNA XIST knockdown suppresses the growth of colorectal cancer cells via regulating microRNA-338-3p/PAX5 axis. Eur J Cancer Prev. 2021;30:132–42.
23. Jiang Q, Xing W, Cheng J, Yu Y. Knockdown of lncRNA XIST Suppresses Cell Tumorigenicity in Human Non-Small Cell Lung Cancer by Regulating miR-142-5p/PAX6 Axis. Onco Targets Ther. 2020;13:4919–29.
24. Yan XT, Lu JM, Wang Y, Cheng XL, He XH, Zheng WZ, et al. XIST accelerates neuropathic pain progression through regulation of miR-150 and ZEB1 in CCI rat models. J Cell Physiol. 2018; 233:6098–106.
25. Krishna BA, Wass AB, O'Connor CM. Activator protein-1 transactivation of the major immediate early locus is a determinant of cytomegalovirus reactivation from latency. Proc Natl Acad Sci USA. 2020;117:20860–7.
26. Matsuoka K, Bakiri L, Wolff LI, Linder M, Mikels-Vigdal A, Patino-Garcia A, et al. Wnt signaling and Loxl2 promote aggressive osteosarcoma. Cell Res. 2020;30:885–901.
27. Rodriguez-Berdini L, Ferrero GO, Bustos Plonka F, Cardozo Gizzi AM, Prucca CG, Quiroga S, et al. The moonlighting protein c-Fos activates lipid synthesis in neurons, an activity that is critical for cellular differentiation and cortical development. J Biol Chem. 2020;295:8808–18.
28. Jancso G, Lantos J, Borsiczky B, Szanto Z, Roth E. Dynamism of NF-kappaB and AP-1 activation in the signal transduction of ischaemic myocardial preconditioning. Eur Surg Res. 2004;36: 129–35.
29. Zhu J, Yao K, Guo J, Shi H, Ma L, Wang Q, et al. miR-181a and miR-150 regulate dendritic cell immune inflammatory responses and cardiomyocyte apoptosis via targeting JAK1-STAT1/c-Fos pathway. J Cell Mol Med. 2017;21:2884–95.
30. Shi J, Gao W, Shao F. Pyroptosis: Gasdermin-mediated programmed necrotic cell death. Trends Biochem Sci. 2017;42:245–54.
31. Li N, Zhou H, Wu H, Wu Q, Duan M, Deng W, et al. STING-IRF3 contributes to lipopolysaccharide-induced cardiac dysfunction, inflammation, apoptosis and pyroptosis by activating NLRP3. Redox Biol. 2019;24:101215.
32. Qiu Z, He Y, Ming H, Lei S, Leng Y, Xia ZY. Lipopolysaccharide (LPS) aggravates high glucose- and hypoxia/reoxygenation-induced injury through activating ROS-dependent NLRP3 inflammasome-mediated pyroptosis in H9C2 cardiomyocytes. J Diabetes Res. 2019;2019:8151836.
33. Hughes MM, O'Neill LAJ. Metabolic regulation of NLRP3. Immunol Rev. 2018;281:88–98.
34. An X, Zhang Y, Cao Y, Chen J, Qin H, Yang L. Punicalagin protects diabetic nephropathy by inhibiting pyroptosis based on TXNIP/NLRP3 pathway. Nutrients. 2020;12:1516.
35. Lian D, Dai L, Xie Z, Zhou X, Liu X, Zhang Y, et al. Periodontal ligament fibroblasts migration injury via ROS/TXNIP/Nlrp3 inflammasome pathway with Porphyromonas gingivalis lipopolysaccharide. Mol Immunol. 2018;103:209–19.
36. Liang D, Jin Y, Lin M, Xia X, Chen X, Huang A. Down-regulation of Xist and Mir-7a-5p improves LPS-induced myocardial injury. Int J Med Sci. 2020;17:2570–7.